Open charm yields in d+Au collisions at $\sqrt{s_{_{NN}}} = 200$ GeV

J. Adams,[3] M.M. Aggarwal,[29] Z. Ahammed,[43] J. Amonett,[20] B.D. Anderson,[20] D. Arkhipkin,[13] G.S. Averichev,[12] S.K. Badyal,[19] Y. Bai,[27] J. Balewski,[17] O. Barannikova,[32] L.S. Barnby,[3] J. Baudot,[18] S. Bekele,[28] V.V. Belaga,[12] R. Bellwied,[46] J. Berger,[14] B.I. Bezverkhny,[48] S. Bharadwaj,[33] A. Bhasin,[19] A.K. Bhati,[29] V.S. Bhatia,[29] H. Bichsel,[45] A. Billmeier,[46] L.C. Bland,[4] C.O. Blyth,[3] B.E. Bonner,[34] M. Botje,[27] A. Boucham,[38] A.V. Brandin,[25] A. Bravar,[4] M. Bystersky,[11] R.V. Cadman,[1] X.Z. Cai,[37] H. Caines,[48] M. Calderón de la Barca Sánchez,[17] J. Castillo,[21] D. Cebra,[7] Z. Chajecki,[44] P. Chaloupka,[11] S. Chattopadhyay,[43] H.F. Chen,[36] Y. Chen,[8] J. Cheng,[41] M. Cherney,[10] A. Chikanian,[48] W. Christie,[4] J.P. Coffin,[18] T.M. Cormier,[46] J.G. Cramer,[45] H.J. Crawford,[6] D. Das,[43] S. Das,[43] M.M. de Moura,[35] A.A. Derevschikov,[31] L. Didenko,[4] T. Dietel,[14] S.M. Dogra,[19] W.J. Dong,[8] X. Dong,[36] J.E. Draper,[7] F. Du,[48] A.K. Dubey,[15] V.B. Dunin,[12] J.C. Dunlop,[4] M.R. Dutta Mazumdar,[43] V. Eckardt,[23] W.R. Edwards,[21] L.G. Efimov,[12] V. Emelianov,[25] J. Engelage,[6] G. Eppley,[34] B. Erazmus,[38] M. Estienne,[38] P. Fachini,[4] J. Faivre,[18] R. Fatemi,[17] J. Fedorisin,[12] K. Filimonov,[21] P. Filip,[11] E. Finch,[48] V. Fine,[4] Y. Fisyak,[4] K. Fomenko,[12] J. Fu,[41] C.A. Gagliardi,[39] L. Gaillard,[3] J. Gans,[48] M.S. Ganti,[43] L. Gaudichet,[38] F. Geurts,[34] V. Ghazikhanian,[8] P. Ghosh,[43] J.E. Gonzalez,[8] O. Grachov,[46] O. Grebenyuk,[27] D. Grosnick,[42] S.M. Guertin,[8] Y. Guo,[46] A. Gupta,[19] T.D. Gutierrez,[7] T.J. Hallman,[4] A. Hamed,[46] D. Hardtke,[21] J.W. Harris,[48] M. Heinz,[2] T.W. Henry,[39] S. Hepplemann,[30] B. Hippolyte,[18] A. Hirsch,[32] E. Hjort,[21] G.W. Hoffmann,[40] H.Z. Huang,[8] S.L. Huang,[36] E.W. Hughes,[5] T.J. Humanic,[28] G. Igo,[8] A. Ishihara,[40] P. Jacobs,[21] W.W. Jacobs,[17] M. Janik,[44] H. Jiang,[8] P.G. Jones,[3] E.G. Judd,[6] S. Kabana,[2] K. Kang,[41] M. Kaplan,[9] D. Keane,[20] V.Yu. Khodyrev,[31] J. Kiryluk,[22] A. Kisiel,[44] E.M. Kislov,[12] J. Klay,[21] S.R. Klein,[21] D.D. Koetke,[42] T. Kollegger,[14] M. Kopytine,[20] L. Kotchenda,[25] M. Kramer,[26] P. Kravtsov,[25] V.I. Kravtsov,[31] K. Krueger,[1] C. Kuhn,[18] A.I. Kulikov,[12] A. Kumar,[29] R.Kh. Kutuev,[13] A.A. Kuznetsov,[12] M.A.C. Lamont,[48] J.M. Landgraf,[4] S. Lange,[14] F. Laue,[4] J. Lauret,[4] A. Lebedev,[4] R. Lednicky,[12] S. Lehocka,[12] M.J. LeVine,[4] C. Li,[36] Q. Li,[46] Y. Li,[41] G. Lin,[48] S.J. Lindenbaum,[26] M.A. Lisa,[28] F. Liu,[47] L. Liu,[47] Q.J. Liu,[45] Z. Liu,[47] T. Ljubicic,[4] W.J. Llope,[34] H. Long,[8] R.S. Longacre,[4] M. Lopez-Noriega,[28] W.A. Love,[4] Y. Lu,[47] T. Ludlam,[4] D. Lynn,[4] G.L. Ma,[37] J.G. Ma,[8] Y.G. Ma,[37] D. Magestro,[28] S. Mahajan,[19] D.P. Mahapatra,[15] R. Majka,[48] L.K. Mangotra,[19] R. Manweiler,[42] S. Margetis,[20] C. Markert,[20] L. Martin,[38] J.N. Marx,[21] H.S. Matis,[21] Yu.A. Matulenko,[31] C.J. McClain,[1] T.S. McShane,[10] F. Meissner,[21] Yu. Melnick,[31] A. Meschanin,[31] M.L. Miller,[22] N.G. Minaev,[31] C. Mironov,[20] A. Mischke,[27] D.K. Mishra,[15] J. Mitchell,[34] B. Mohanty,[43] L. Molnar,[32] C.F. Moore,[40] D.A. Morozov,[31] M.G. Munhoz,[35] B.K. Nandi,[43] S.K. Nayak,[19] T.K. Nayak,[43] J.M. Nelson,[3] P.K. Netrakanti,[43] V.A. Nikitin,[13] L.V. Nogach,[31] S.B. Nurushev,[31] G. Odyniec,[21] A. Ogawa,[4] V. Okorokov,[25] M. Oldenburg,[21] D. Olson,[21] S.K. Pal,[43] Y. Panebratsev,[12] S.Y. Panitkin,[4] A.I. Pavlinov,[46] T. Pawlak,[44] T. Peitzmann,[27] V. Perevoztchikov,[4] C. Perkins,[6] W. Peryt,[44] V.A. Petrov,[13] S.C. Phatak,[15] R. Picha,[7] M. Planinic,[49] J. Pluta,[44] N. Porile,[32] J. Porter,[45] A.M. Poskanzer,[21] M. Potekhin,[4] E. Potrebenikova,[12] B.V.K.S. Potukuchi,[19] D. Prindle,[45] C. Pruneau,[46] J. Putschke,[23] G. Rakness,[30] R. Raniwala,[33] S. Raniwala,[33] O. Ravel,[38] R.L. Ray,[40] S.V. Razin,[12] D. Reichhold,[32] J.G. Reid,[45] G. Renault,[38] F. Retiere,[21] A. Ridiger,[25] H.G. Ritter,[21] J.B. Roberts,[34] O.V. Rogachevskiy,[12] J.L. Romero,[7] A. Rose,[46] C. Roy,[38] L. Ruan,[36] R. Sahoo,[15] I. Sakrejda,[21] S. Salur,[48] J. Sandweiss,[48] M. Sarsour,[17] I. Savin,[13] P.S. Sazhin,[12] J. Schambach,[40] R.P. Scharenberg,[32] N. Schmitz,[23] K. Schweda,[21] J. Seger,[10] P. Seyboth,[23] E. Shahaliev,[12] M. Shao,[36] W. Shao,[5] M. Sharma,[29] W.Q. Shen,[37] K.E. Shestermanov,[31] S.S. Shimanskiy,[12] E Sichtermann,[21] F. Simon,[23] R.N. Singaraju,[43] G. Skoro,[12] N. Smirnov,[48] R. Snellings,[27] G. Sood,[42] P. Sorensen,[21] J. Sowinski,[17] J. Speltz,[18] H.M. Spinka,[1] B. Srivastava,[32] A. Stadnik,[12] T.D.S. Stanislaus,[42] R. Stock,[14] A. Stolpovsky,[46] M. Strikhanov,[25] B. Stringfellow,[32] A.A.P. Suaide,[35] E. Sugarbaker,[28] C. Suire,[4] M. Sumbera,[11] B. Surrow,[22] T.J.M. Symons,[21] A. Szanto de Toledo,[35] P. Szarwas,[44] A. Tai,[8] J. Takahashi,[35] A.H. Tang,[27] T. Tarnowsky,[32] D. Thein,[8] J.H. Thomas,[21] S. Timoshenko,[25] M. Tokarev,[12] T.A. Trainor,[45] S. Trentalange,[8] R.E. Tribble,[39] O.D. Tsai,[8] J. Ulery,[32] T. Ullrich,[4] D.G. Underwood,[1] A. Urkinbaev,[12] G. Van Buren,[4] M. van Leeuwen,[21] A.M. Vander Molen,[24] R. Varma,[16] I.M. Vasilevski,[13] A.N. Vasiliev,[31] R. Vernet,[18] S.E. Vigdor,[17] Y.P. Viyogi,[43] S. Vokal,[12] S.A. Voloshin,[46] M. Vznuzdaev,[25] W.T. Waggoner,[10] F. Wang,[32] G. Wang,[20] G. Wang,[5] X.L. Wang,[36] Y. Wang,[40] Y. Wang,[41] Z.M. Wang,[36] H. Ward,[40] J.W. Watson,[20] J.C. Webb,[17] R. Wells,[28]

G.D. Westfall,[24] A. Wetzler,[21] C. Whitten Jr.,[8] H. Wieman,[21] S.W. Wissink,[17] R. Witt,[2] J. Wood,[8] J. Wu,[36] N. Xu,[21] Z. Xu,[4] Z.Z. Xu,[36] E. Yamamoto,[21] P. Yepes,[34] V.I. Yurevich,[12] Y.V. Zanevsky,[12] H. Zhang,[4] W.M. Zhang,[20] Z.P. Zhang,[36] R. Zoulkarneev,[13] Y. Zoulkarneeva,[13] and A.N. Zubarev[12]
(STAR Collaboration)

[1]*Argonne National Laboratory, Argonne, Illinois 60439*
[2]*University of Bern, 3012 Bern, Switzerland*
[3]*University of Birmingham, Birmingham, United Kingdom*
[4]*Brookhaven National Laboratory, Upton, New York 11973*
[5]*California Institute of Technology, Pasadena, California 91125*
[6]*University of California, Berkeley, California 94720*
[7]*University of California, Davis, California 95616*
[8]*University of California, Los Angeles, California 90095*
[9]*Carnegie Mellon University, Pittsburgh, Pennsylvania 15213*
[10]*Creighton University, Omaha, Nebraska 68178*
[11]*Nuclear Physics Institute AS CR, 250 68 Řež/Prague, Czech Republic*
[12]*Laboratory for High Energy (JINR), Dubna, Russia*
[13]*Particle Physics Laboratory (JINR), Dubna, Russia*
[14]*University of Frankfurt, Frankfurt, Germany*
[15]*Institute of Physics, Bhubaneswar 751005, India*
[16]*Indian Institute of Technology, Mumbai, India*
[17]*Indiana University, Bloomington, Indiana 47408*
[18]*Institut de Recherches Subatomiques, Strasbourg, France*
[19]*University of Jammu, Jammu 180001, India*
[20]*Kent State University, Kent, Ohio 44242*
[21]*Lawrence Berkeley National Laboratory, Berkeley, California 94720*
[22]*Massachusetts Institute of Technology, Cambridge, MA 02139-4307*
[23]*Max-Planck-Institut für Physik, Munich, Germany*
[24]*Michigan State University, East Lansing, Michigan 48824*
[25]*Moscow Engineering Physics Institute, Moscow Russia*
[26]*City College of New York, New York City, New York 10031*
[27]*NIKHEF, Amsterdam, The Netherlands*
[28]*Ohio State University, Columbus, Ohio 43210*
[29]*Panjab University, Chandigarh 160014, India*
[30]*Pennsylvania State University, University Park, Pennsylvania 16802*
[31]*Institute of High Energy Physics, Protvino, Russia*
[32]*Purdue University, West Lafayette, Indiana 47907*
[33]*University of Rajasthan, Jaipur 302004, India*
[34]*Rice University, Houston, Texas 77251*
[35]*Universidade de Sao Paulo, Sao Paulo, Brazil*
[36]*University of Science & Technology of China, Anhui 230027, China*
[37]*Shanghai Institute of Applied Physics, Shanghai 201800, China*
[38]*SUBATECH, Nantes, France*
[39]*Texas A&M University, College Station, Texas 77843*
[40]*University of Texas, Austin, Texas 78712*
[41]*Tsinghua University, Beijing 100084, China*
[42]*Valparaiso University, Valparaiso, Indiana 46383*
[43]*Variable Energy Cyclotron Centre, Kolkata 700064, India*
[44]*Warsaw University of Technology, Warsaw, Poland*
[45]*University of Washington, Seattle, Washington 98195*
[46]*Wayne State University, Detroit, Michigan 48201*
[47]*Institute of Particle Physics, CCNU (HZNU), Wuhan 430079, China*
[48]*Yale University, New Haven, Connecticut 06520*
[49]*University of Zagreb, Zagreb, HR-10002, Croatia*

(Dated: February 7, 2008)

Mid-rapidity open charm spectra from direct reconstruction of $D^0(\overline{D^0}) \rightarrow K^{\mp}\pi^{\pm}$ in d+Au collisions and indirect electron/positron measurements via charm semileptonic decays in p+p and d+Au collisions at $\sqrt{s_{\rm NN}}$= 200 GeV are reported. The $D^0(\overline{D^0})$ spectrum covers a transverse momentum (p_T) range of $0.1 < p_T < 3$ GeV/c whereas the electron spectra cover a range of $1 < p_T < 4$ GeV/c. The electron spectra show approximate binary collision scaling between p+p and d+Au collisions. From these two independent analyses, the differential cross section per nucleon-nucleon binary interaction at mid-rapidity for open charm production from d+Au collisions at RHIC is $d\sigma^{NN}_{c\bar{c}}/dy$=0.30±0.04 (stat.)±0.09(syst.) mb. The results are compared to theoretical calculations. Implications for charmoniumm results in A+A collisions are discussed.

PACS numbers: 25.75.Dw, 13.20.Fc, 13.25.Ft, 24.85.+p

Hadrons with heavy flavor are unique tools for studying the strong interaction described by Quantum Chromodynamics (QCD). Due to the large mass of the charm quark ($\sim$ 1.5 GeV/c^2), charm quark production can be evaluated by perturbative QCD (pQCD) even at low momentum through the introduction of additional scales related to the charm quark mass [1, 2]. Therefore, theoretical calculation of charm hadron total cross section integrated over momentum space is expected to be less affected by non-perturbative soft processes and hadronization [3]. Systematic studies of charm production in p+p and p+nucleus collisions have been proposed as a sensitive way to measure the parton distribution function in nucleons, and nuclear shadowing effects [4]. At RHIC energies, heavy quark energy loss [5], charm quark coalescence [6, 7, 8, 9], possible J/ψ suppression [10], and charm flow [11] have been proposed as important tools in studying the properties of matter created in heavy ion collisions.

Identification of charmed hadrons is difficult due to their short lifetime ($c\tau(D^0)$ = 124 μm), low production rates, and large combinatorial background. Most measurements of the total charm cross section in hadron-hadron collisions have been performed at low center-of-mass energies ($\lesssim$ 40 GeV) in fixed target experiments [12, 13]. At $\sqrt{s} \sim 52 - 63$ GeV, the available measurements are not conclusive due to inconsistencies between different measurements [12, 14]. The measurements at higher energy colliders have been at high p_T only [15] , or have included large uncertainties [16, 17]. Theoretical predictions for the RHIC energy region differ significantly [18, 19]. Therefore, precise measurements of charm cross sections in p+p and d+Au collisions in this energy region are crucial. In this paper, we report first results on open charm cross sections at $\sqrt{s_{_{\rm NN}}}$= 200 GeV from direct charmed hadron $D^0(\overline{D^0})$ reconstruction in d+Au collisions and from charm semileptonic decay in both p+p and d+Au collisions. These measurements are complementary, providing important experimental cross-checks.

The data used in D^0 direct reconstruction and charm semileptonic decay analysis were taken during the 2003 RHIC run in d+Au and p+p collisions at $\sqrt{s_{_{\rm NN}}}$= 200 GeV with the Solenoidal Tracker at RHIC (STAR). A minimum bias d+Au collision trigger was defined by requiring at least one spectator neutron in the outgoing Au beam direction depositing energy in a Zero Degree Calorimeter (ZDC). Detailed descriptions of the trigger and centrality definition in d+Au collisions have been presented in a previous publication [20]. A total of 15.7 million minimum bias triggered d+Au collision events were used in the D^0 analysis. The data samples used in the electron analysis in d+Au and p+p collisions were described in Ref. [21]. The integrated luminosity is about 40 μb^{-1} for d+Au collisions and 30 nb^{-1} for p+p collisions.

The primary tracking device of the STAR detector is the Time Projection Chamber (TPC) [22]. It was used to reconstruct the decay of $D^0 \rightarrow K^-\pi^+$ ($\overline{D^0} \rightarrow K^+\pi^-$) which has a branching ratio of 3.83%. In what follows, we imply $(D^0+\overline{D^0})/2$ when using the term D^0 unless otherwise specified. The exact D^0 decay topology cannot be resolved due to insufficient track projection resolution close to the collision vertex. The invariant mass spectrum of D^0 mesons was obtained by pairing each oppositely charged kaon and pion candidate in the same event. The kaon and pion tracks were identified through ionization energy loss (dE/dx) in the TPC wherever the identification is possible. Candidate tracks were selected having momenta p (p_T) $>$ 0.3 (0.2) GeV/c and pseudorapidity $|\eta| < 1$. The D^0 signal with $p_T < 3$ GeV/c and $|y| < 1$ after mixed-event background subtraction [23] is shown in the left panel of Fig. 1. The signal-to-background ratio (S/N) is about 1/600, and the figure of merit ($S/\sqrt{N}$) is about 6. This distribution was fit to a Gaussian plus a linear function to account for the residual background not described by the mixed-event spectrum [23]. The open symbols in the left panel of Fig. 1 depict the D^0 signal after the two-step background subtraction. HIJING simulations [24] have shown that di-hadron correlations from jets can affect the line-shape of the background spectrum since the shape (slope versus mass) from this contribution is different from that of random pairs. To estimate the uncertainty in the subtraction of the residual background, different normalizations, slopes and fit ranges were tried. The resulting uncertainty in the D^0 yield is estimated to be 15%. Within statistical uncertainties, the yields of D^0 and $\overline{D^0}$ are equal. The $D^0 \rightarrow K^-\pi^+$ signal could be mis-identified as a $\overline{D^0} \rightarrow K^+\pi^-$ and vice versa when both of its daughters are beyond particle identification in the TPC. This misidentification results in double counting which was corrected for in the D^0 yields through a Monte Carlo simulation.

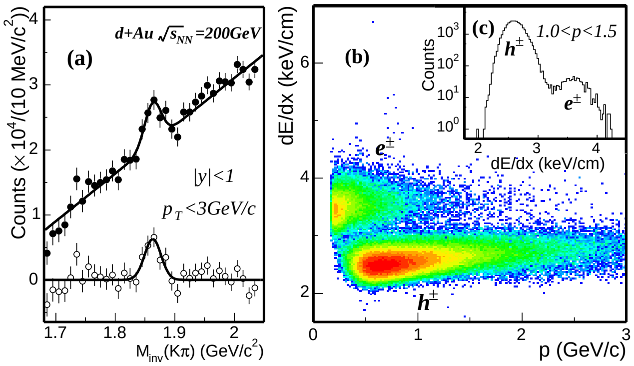

FIG. 1: (a) Invariant mass distributions of kaon-pion pairs from d+Au collisions. The solid circles depict the signal after mixed-event background subtraction, the open circles after subtraction of the residual background using a linear parametrization. (b) dE/dx in the TPC vs. particle momentum (p) with a TOF cut of $|1/\beta - 1| \leq 0.03$. Insert: projection on the dE/dx axis for particle momenta $1< p <1.5$ GeV/c.

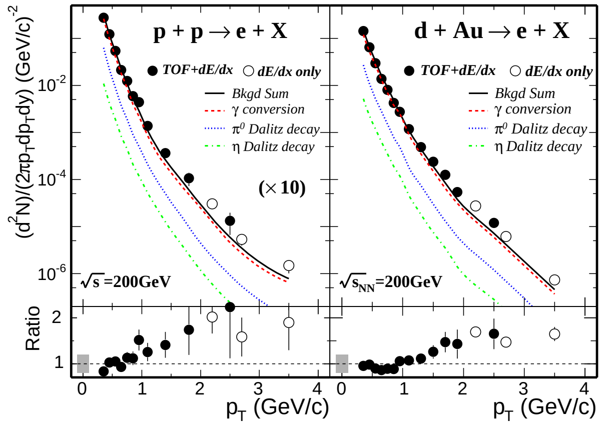

FIG. 2: Upper panels: Electron distributions from p+p (left) and d+Au (right) collisions. Solid and open symbols depict electrons/positrons $((e^+ + e^-)/2)$ identified via a combination of Time-of-Flight (TOF) and dE/dx, and electrons (e^-) identified via dE/dx alone. The total photonic backgrounds are shown as solid lines. Dashed lines depict the various contributing sources. The fractions were derived from simulations. Bottom panels: the ratio of inclusive electrons to the total backgrounds. The gray band represents the systematic uncertainty in each panel.

Another detector used in this analysis was a prototype time-of-flight system (TOFr) [25] based on multi-gap resistive plate chamber technology. It covers an azimuthal angle $\Delta\phi \simeq \pi/30$, and $-1 < \eta < 0$. In addition to its hadron identification capability [21], it allows electrons/positrons to be identified at low momentum ($p_T < 3$ GeV/c) by using a combination of velocity information (β) from TOFr and dE/dx measured in the TPC. The right panel of Fig. 1 demonstrates the clean separation of electrons from hadrons using their dE/dx in the TPC after applying a TOFr cut of $|1/\beta - 1| \leq 0.03$. This cut eliminated the hadrons crossing the electron dE/dx band. Electrons/positrons were required to originate from the collision vertex. Hadron contamination was evaluated to be about $10 - 15\%$ in a selection optimized for purity and statistics. At higher p_T ($2 - 4$ GeV/c), electrons could be identified directly in the TPC since hadrons have lower dE/dx due to the relativistic rise of the dE/dx for electrons. Positrons are more difficult to identify using dE/dx alone because of the large background from the deuteron band. The hadron contamination in this case was found to be $\lesssim 5\%$ at $p_T \simeq 2$ GeV/c and to increase to $\sim 30\%$ at $p_T \simeq 3-4$ GeV/c. This was corrected for in the final spectra. Detector acceptance and efficiency corrections were determined from detailed simulations [21]. Total inclusive electron spectra from 200 GeV p+p and d+Au collisions are shown in Fig. 2.

Gamma conversions $\gamma \rightarrow e^+e^-$ and $\pi^0 \rightarrow \gamma e^+e^-$ Dalitz decays are the dominant photonic sources of electron background. To measure the background photonic electron spectra, the invariant mass and opening angle of the e^+e^- pairs were constructed from an electron (positron) in TOFr and every other positron (electron) candidate reconstructed in the TPC [26]. A secondary vertex at the conversion point was not required. Simulations with both HIJING [24] and PYTHIA [27] with full detector description in GEANT yielded $\sim 60\%$ efficiency for electrons with $p_T > 1$ GeV/c from such background processes. More than 95% of the electrons from sources other than heavy-flavor semileptonic decays were measured with this method. The remaining fraction from decays of η, ω, ρ, ϕ and K was determined from simulations. The results are shown as solid lines in Fig. 2. The overall uncertainty of the background is on the order of 20% and has been included in the systematic errors. Ratios of the inclusive electrons over the total backgrounds are shown in the bottom panels of Fig. 2. The signal is clearly in excess of the background above $p_T > 1$ GeV/c.

The non-photonic electron spectra were obtained by subtracting the previously described photonic background from the inclusive spectra. The results are shown in Fig. 3. The D^0 invariant yields $d^2N/(2\pi p_T dp_T dy)$ as a function of p_T from direct reconstruction are shown in Fig. 3 as solid squares. Two different fitting methods were used to extract dN/dy for the D^0 at mid-rapidity. In the first method, dN/dy was extracted from an exponential fit to the D^0 differential yield in transverse mass

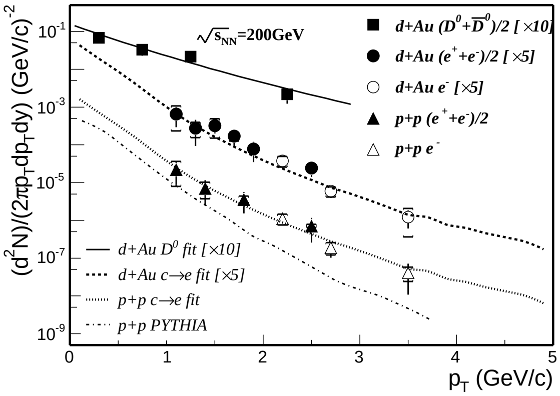

FIG. 3: Reconstructed D^0 (solid squares) p_T distributions from d+Au collisions at $\sqrt{s_{NN}} = 200$ GeV. Non-photonic electron p_T distributions from p+p collisions (triangles) and d+Au collisions (circles). Solid and dashed lines are the fit results from both D^0 and electron spectra in d+Au collisions. The dotted line is scaled down by a factor of $N_{bin} = 7.5 \pm 0.4$ [20] from d+Au to p+p collisions. The dot-dashed line depicts a PYTHIA calculation [27].

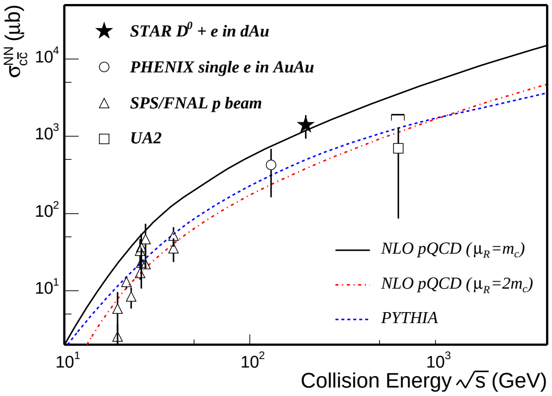

FIG. 4: Total $c\bar{c}$ cross section per nucleon-nucleon collision vs. the collision energy ($\sqrt{s_{\rm NN}}$). The dashed line depicts a PYTHIA calculation [27]. The solid and dot-dashed lines depict two NLO pQCD calculations with MRST HO, $m_c = 1.2$ GeV/c^2, $\mu_F = 2m_c$, $\mu_R = m_c$ and $2m_c$, respectively [18].

(m_T) [23]. In the second method, a simultaneous fit was applied to both directly reconstructed D^0's and the background subtracted non-photonic electron distribution in d+Au collisions. For this fit, it was assumed that the D^0 spectrum follows a power law in p_T from which an electron spectrum was generated using the particle composition from [28] and the decay generators in PYTHIA. A set of parameters for the power law was found at the minimum of χ^2 for the D^0 and electron spectra. The results are shown in Table I. The systematic error is dominated by the uncertainties in the background subtraction, the extrapolation due to finite p_T coverage, and the overall normalization (±14% in p+p and ±10% in d+Au collisions [20, 21]).

The yield of D^0 at mid-rapidity is $dN/dy = 0.028 \pm 0.004 \pm 0.008$ and the $\langle p_T \rangle = 1.32 \pm 0.08$ GeV/c in d+Au collisions. We used the ratio $R = N_{D^0}/N_{c\bar{c}} = 0.54 \pm 0.05$ from e^+e^- collider data [28] to convert the D^0 yield to a total $c\bar{c}$ yield. A p+p inelastic scattering cross section of $\sigma_{inel}^{pp} = 42$ mb was used in the calculation and a factor of $f = 4.7 \pm 0.7$, estimated from simulation [18, 27], was used to convert the $d\sigma/dy$ at mid-rapidity to the total cross section. The total charm cross section per nucleon-nucleon interaction for d+Au collisions at 200 GeV is $\sigma_{c\bar{c}}^{NN} = dN_{D^0}^{d+Au}/dy \times \sigma_{inel}^{pp}/N_{bin}^{d+Au} \times f/R = 1.3 \pm 0.2 \pm 0.4$ mb from D^0 alone and $1.4 \pm 0.2 \pm 0.4$ mb from the combined fit of D^0 and electrons. The nuclear modification factor [20] was obtained by taking the ratio of the electron spectra in d+Au and p+p collisions scaled with the underlying nucleon-nucleon binary collisions. It was measured to be $1.3 \pm 0.3 \pm 0.3$, averaged over $1 < p_T < 4$ GeV/c. This value is consistent with binary scaling within the measured errors.

	$dN(D^0)/dy\vert_{y=0}$ (10^{-2})	$d\sigma_{c\bar{c}}^{NN}/dy\vert_{y=0}$ (mb)
D^0	2.8±0.4±0.8	0.29±0.04±0.08
$D^0+e^\pm$	2.9±0.4±0.8	0.30±0.04±0.09

TABLE I: dN/dy of D^0 in d+Au collisions and the corresponding $d\sigma/dy$ of $c\bar{c}$ pair per nucleon-nucleon collision at $\sqrt{s_{\rm NN}}$= 200 GeV.

The beam energy dependence of the cross section is shown in Fig. 4. Both default PYTHIA [27] and NLO pQCD [18] calculations reasonably describe the results at lower energies, but underpredict the total charm cross section at $\sqrt{s_{NN}} = 200$ GeV. A NLO pQCD calculation (solid line) with fragmentation and renormalization scales chosen to be $\mu_F = 2m_c$ and $\mu_R = m_c$ ($m_c = 1.2$ GeV/c^2) reproduces our result. The underprediction by PYTHIA of the charm cross section is also evident in Fig. 3 , the charm decayed electron p_T distribution shown as dot-dashed line. Furthermore, the slope of the PYTHIA distributions is much steeper than the measured distribution. There are also indications that a large charm production cross section at $\sqrt{s_{NN}} \simeq 300$ GeV is essential to explain available cosmic ray data [29].

At RHIC energies, binary scaling of the open charm production is expected between p+p, p+A and A+A collisions [4]. If correct, the results of this study suggest a much larger charm yield in central Au+Au collisions than previously assumed in statistical thermal models [7, 8, 9] based on some pQCD/PYTHIA calculations. This would rule out several predictions [7, 8, 9] of charm production not previously excluded by the upper limit (below binary scaling) set by J/ψ production in central Au+Au collisions [30]. Future heavy ion runs at RHIC with open charm and J/ψ measurements will enable us to study the flow and thermalization of charmed particles.

In summary, the charm cross section and transverse momentum distribution for p+p and d+Au collisions at $\sqrt{s_{\rm NN}}$= 200 GeV have been measured by the STAR collaboration at RHIC. Independent measurements of the reconstructed D^0 and single electrons from charm semileptonic decay are consistent. The total cross section at this energy was compared to theoretical calculations. The result has important consequences for charm quark coalescence in Au+Au collisions at RHIC.

We are grateful for many fruitful discussions with D. Kharzeev, and R. Vogt. We thank the RHIC Operations Group and RCF at BNL, and the NERSC Center at LBNL for their support. This work was supported in part by the HENP Divisions of the Office of Science of the U.S. DOE; the U.S. NSF; the BMBF of Germany; IN2P3, RA, RPL, and EMN of France; EPSRC of the United Kingdom; FAPESP of Brazil; the Russian Ministry of Science and Technology; the Ministry of Education and the NNSFC of China; Grant Agency of the Czech Republic, FOM and UU of the Netherlands, DAE, DST, and CSIR of the Government of India; Swiss NSF; and the Polish State Committee for Scientific Research.

---

[1] P.L. McGaughey *et al.*, *Int. J. Mod. Phys.* A **10**, 2999 (1995).
[2] M.L. Mangano *et al.*, *Nucl. Phys.* B **405**, 507 (1993).
[3] B.A. Kniehl *et al.*, *Nucl. Phys.* B **597**, 337 (2001); S. Kretzer, *Phys. Rev.* D **62**, 054001 (2000).
[4] Z. Lin and M. Gyulassy, *Phys. Rev. Lett.* **77**, 1222 (1996).
[5] Y.L. Dokshitzer and D.E. Kharzeev, *Phys. Lett.* B **519**, 199 (2001).
[6] L. Grandchamp and R. Rapp, *Phys. Lett.* B **523**, 60 (2001).
[7] A. Andronic *et al.*, *Phys. Lett.* B **571**, 36 (2003).
[8] R.L. Thews, M. Schroedter, and J. Rafelski, *Phys. Rev.* C **63**, 054905 (2001).
[9] M.I. Gorenstein *et al.*, *J. Phys.* G **28**, 2151 (2002).
[10] T. Matsui and H. Satz, *Phys. Lett.* B **178**, 416 (1986).
[11] S. Batsouli *et al.*, *Phys. Lett.* B **557**, 26 (2003); Z.W. Lin and D. Molnar, *Phys. Rev.* C **68**, 044901 (2003); V. Greco, C.M. Ko and R. Rapp, *Phys. Lett.* B **595**, 202 (2004); X. Dong *et al.*, *Phys. Lett.* B **597**, 328 (2004).
[12] S.P.K. Tavernier, *Rep. Prog. Phys.* **50**, 1439 (1987). Total cross sections extrapolated from very high x_F and/or from correlations with low acceptance are not included in Fig.4.
[13] G.A. Alves *et al.* (E769 Collaboration), *Phys. Rev. Lett.* **77**, 2388 (1996).
[14] F.W. Büsser *et al.*, *Nucl. Phys.* B **113**, 189 (1976).
[15] D. Acosta *et al.* (CDF II Collaboration), *Phys. Rev. Lett.* **91**, 241804 (2003).
[16] K. Adcox *et al.* (PHENIX Collaboration), *Phys. Rev. Lett.* **88**, 192303 (2002).
[17] O. Botner *et al.*, *Phys. Lett.* B **236**, 488 (1990).
[18] R. Vogt, *Int. J. Mod. Phys.* E **12**, 211 (2003); R. Vogt, hep-ph/0203151.
[19] J. Raufeisen and J.-C. Peng, *Phys. Rev.* D **67**, 054008 (2003).
[20] J. Adams *et al.* (STAR Collaboration), *Phys. Rev. Lett.* **91**, 072304 (2003).
[21] J. Adams *et al.* (STAR Collaboration), nucl-ex/0309012.
[22] M. Anderson *et al.*, *Nucl. Instr. Meth.* A **499**, 659 (2003).
[23] C. Adler *et al.* (STAR Collaboration), *Phys. Rev.* C **66**, 061901(R) (2002); H. Zhang, Ph.D. thesis, Yale University, 2003.
[24] X.N. Wang and M. Gyulassy, *Phys. Rev.* D **44**, 3501 (1991).
[25] B. Bonner *et al.*, *Nucl. Instr. Meth.* A **508**, 181 (2003); M. Shao *et al.*, *Nucl. Instr. Meth.* A **492**, 344 (2002).
[26] J. Adams *et al.* (STAR Collaboration), *Phys. Rev.* C **70**, 044902 (2004); I. Johnson, Ph.D. thesis, U.C. Davis, 2002.
[27] T. Sjöstrand *et al.*, Computer Physics Commun. **135**, 238 (2001). PYTHIA 6.152 was used with the parameter settings: MSEL=1, CTEQ5M1. Bottom contribution was estimated to be 20-30% in p_T=2-3 GeV/c, 40-50% in 3-4 GeV/c to the total non-photonic electrons, and negligible at lower p_T.
[28] K. Hagiwara *et al.*, *Phys. Rev.* D **66**, 010001-256 (2002) (Particle Data Group). $N_{D^0}/N_{c\bar{c}}$ was derived from the measured open charm states in e^+e^- at $\sqrt{s}$ = 91 GeV. There is a 10% uncertainty taken into account in the branching ratios of open charm semileptonic decays used in the electron-to-charm fit, reflecting unknown production and branching rations for individual states. The ratio in hadronic production, although somewhat reduced, is consistent with that in e^+e^- within errors.
[29] I.V. Rakobolskaya *et al.*, *Nucl. Phys.* B **122**, 353 (2003) (Proc. Suppl.).
[30] S.S. Adler *et al.* (PHENIX Collaboration), *Phys. Rev.* C **69**, 014901 (2004); S.S. Adler *et al.* (PHENIX Collaboration), *Phys. Rev. Lett.* **92**, 051802 (2004).